Canadian Journal of Pure and Applied Sciences
Vol. 15, No. 1, pp. 5133-5140, Feb 2021
Online ISSN: 1920-3853; Print ISSN: 1715-9997
Available online at www.cjpas.net

Canadian Journal of pure & applied sciences

REFRACTIVE INDEX, A KEY TO BETTER PETROGRAPHY AND TO FUNDAMENTAL LAWS OF NATURE; *m*, *E*, AND *W* VACUUM-STRUCTURE REST-MASS CALCULATIONS

Stephen Arthur Langford
Langford Consulting, Danielson, Connecticut, USA

ABSTRACT

In 1961, in several closely spaced personal communications, our Geology Professor, Dr. Gerald P. Brophy, taught that Mineralogists were ignoring refractive indices (RIs) to their own disadvantage, Geochemists were ignoring optical data, and (almost in the same breath) some subjects had been completely removed from the literature; as if Becke lines were not enough to get me hooked! I asked whether useful RI data might be generated by not optically orienting any fragment; but, instead, ignoring their orientations and quickly counting each randomly-encountered one as of Lesser, Equal, or Greater RI than that of the immersion liquid. "Maybe, with the help of statistical analysis", he replied. This research paper reports sporadic work done since then, to learn how much can be discovered about a rock sample, via an RI-counting technique that could be employed even by K-12 students using simple, inexpensive microscopes and polarizing films; though better equipment would yield better precision and accuracy. The approach should be automated. Calculations of vacuum-structure mass (*m*), energy (*E*), and weight (*W*) are presented.

Keywords: Vacuum Structure, de Broglie, rest mass, energy, weight, RI, permittivity, permeability.

INTRODUCTION

This paper focuses upon work done since my Ph.D. dissertation (Langford, 1972), employing polarized visible light and the liquid-immersion, double-variation method (Emmons, 1943) (but Universal-stage aspects are irrelevant to the present paper) of varying liquid RIs, by changing setup temperatures and/or wavelengths. The 100 liquids employed in this study were calibrated using a modified Jelley refractometer (Langford, 1991). The freshest (least weathered) coarse-grained rock sample that I found on Maui, Hawai'i, is a gabbro (course-grained basalt) dubbed "FUD27". It was collected from the stock at Ukumehame Gulch, West Maui.

Long after completing the data-collection phase (between 23 October 1977 and 11 November 1993) of the present work, the author found that Dr. Gordon A. Macdonald (Chairman of my Dissertation Committee and famed for his beautiful petrographic descriptions) had described (Macdonald, 1942) a sample from the same outcrop from which I drew FUD27: "The olivine gabbro of the stock at 1,600 feet altitude in Ukumehame Canyon is a dark-gray, dense granitic rock with an average grain size of 1.5 mm. The rock is composed of subhedral to anhedral crystals of plagioclase (55%); pale-brown, largely anhedral grains of pigeonite (30%); anhedral grains of olivine (5%); iron ore (4%); and interstitial alkalic feldspar (6%). The pigeonite has an optic angle of 15° to 45°. The plagioclase crystals contain cores of calcic to intermediate labradorite surrounded by strongly zoned shells in which the composition grades to andesine at the outside. Acicular crystals of apatite are enclosed in the interstitial feldspar, which consists of both albite (+ 2 V = 75°) and sanidine (– 2 V = small). The albite is considerably more abundant than the sanidine. Typically, the sanidine and albite are intergrown as antiperthite. A few minute wedge-shaped grains resemble tridymite."

More background information is available: Bulk-chemical analysis (courtesy Dr. Macdonald) of FUD27 (Langford, 1972, page 36, column 1), three manuscripts at https://tinyurl.com/y6kz7yfd, recent preprint (unpublished after Covid-19 closed publisher's offices) at https://tinyurl.com/yyrreo2h, and copious related postings at https://tinyurl.com/to8tsbt (for which, please first read https://tinyurl.com/2vrxk2sy).

THE DATA AND SAMPLING PATTERN

Raw Data are presented in https://tinyurl.com/yxo2dyww. Figure 1 presents the sampling pattern.

Corresponding author e-mail: gambist@gmail.com

In addition to concentrated collection along the D and D1 Fraunhofer lines, data were concentrated along the 580 nm and 600 nm wavelengths, as well as in the parallelopiped between about RIs1.635-1.675 and wavelengths 575 nm to 605 nm. Use of the variable monochromator made Emmons's double-variation method complete, prior work (Langford, 1972, 1982) having been done with either a sodium vapor lamp (D = 589.3 nm) or a dichroic filter (D1 = 589.6 nm). Additionally, sparser regions reflect an effort to examine whether data taken at regions far from the Fraunhofer D line could be successfully projected, parallel to the Wavelength ordinate, back to that line; that was found to be a dangerous practice. Some concentrated data were also patterned in order efficiently to learn as much as possible about both the Salic-mineral and Femic-mineral regions. Because many of the data points were so closely spaced as to seem to be one point, trying to count 698 cases in the figure is a fruitless endeavor.

a sample from the same stock could be found via RI data alone.

Please note in particular that the entire range of Plagioclase-Feldspar RIs (reflective of their chemical compositions) is found in this sample. No known previous work has yielded so comprehensive a reflection of chemical variability in a whole-rock study, whatever may have been the employed technology.

During plane-polarized, liquid-immersion refractometry, when liquid RIs match those of powder fragments (which are sometimes called particles; *ne pas confondre* the virtual particles of Quantum Mechanics), the fragments disappear (Saylor, 1935). Not only that, results show that resonances can be so strong that everything but some opaque fragments can disappear. The author has dubbed that phenomenon "Symphonic Resonance"; it is why we see through the model in various places.

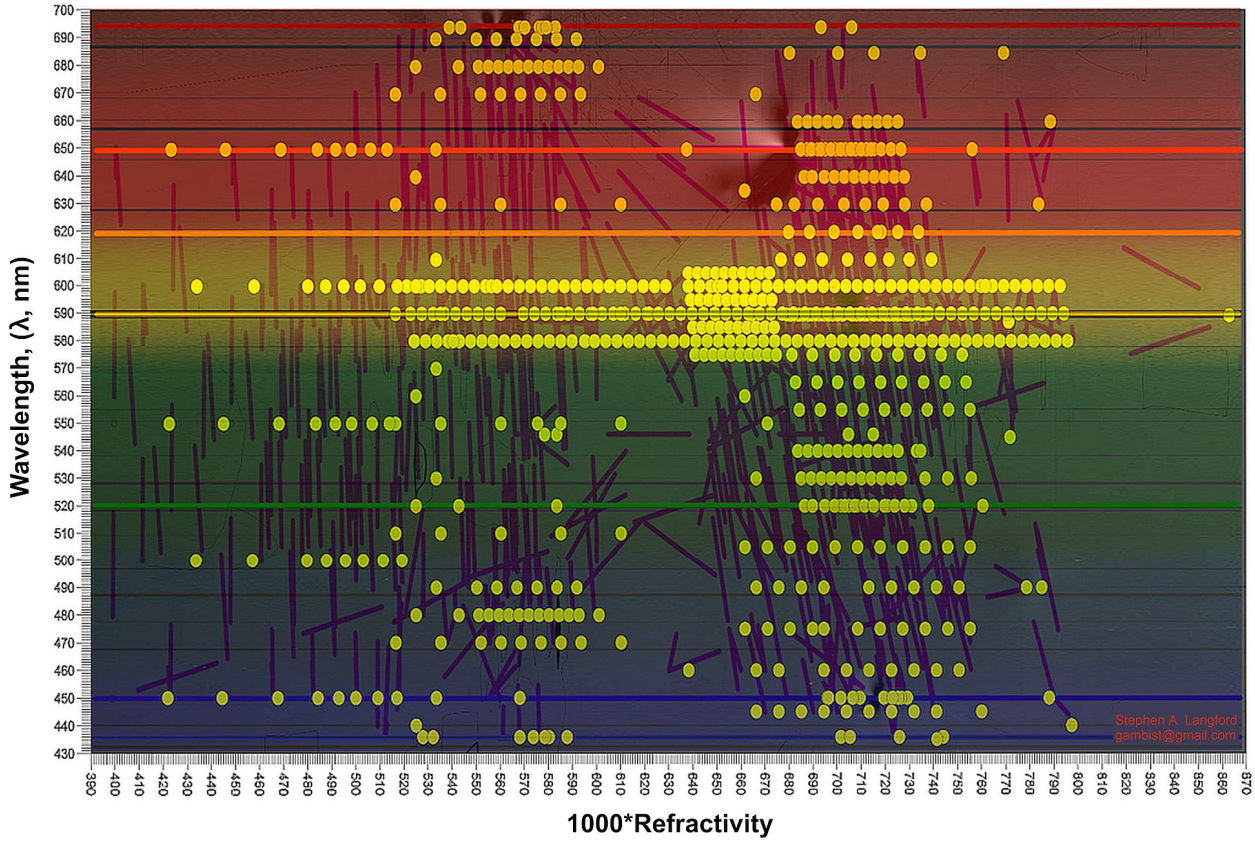

Fig. 1. The 698-case sampling pattern concentrates upon the Fraunhofer Sodium (Na) D line and surrounding region; especially, D1, due to use of a 589.6 nm dichroic filter in place during early work. In later work, wavelengths were set via Optometrics DMC1-03 variable monochromator SN002220 (calibrated at 1 nm/division, with rotatable diffraction grating and a dial that can be read to ~ 0.1 nm increments).

RESULTS AND DISCUSSION

Figure 2 shows two separate profiles exploring which of the minerals mentioned in Dr. Macdonald's description of

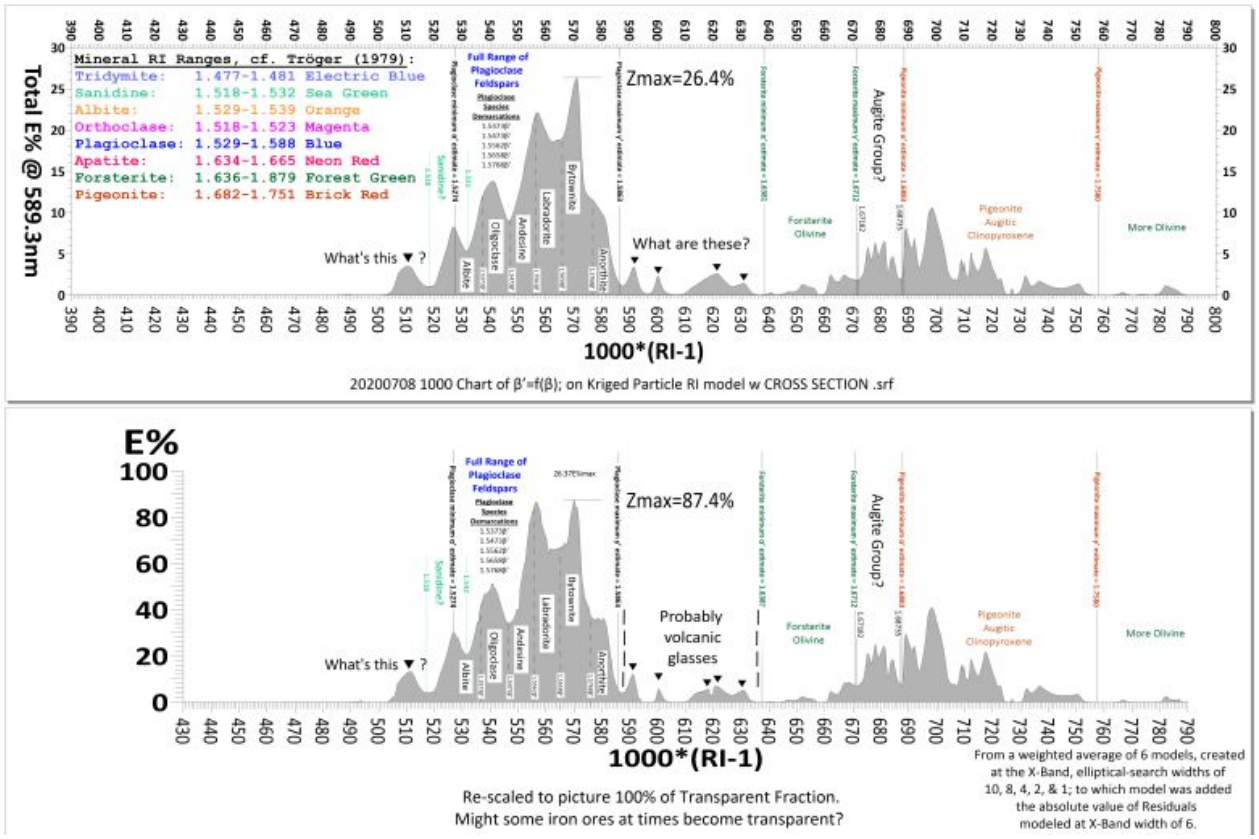

Fig. 2. For the minerals mentioned by Dr. Macdonald, color-coded mineral names and their RI ranges are drawn at two separate Z scales. The lower image involved much-more-extensive modeling efforts than the upper one did, which is reflected in the slightly greater detail of the lower profile. Some classical Optical Mineralogy would be required to identify what causes the hump at RI1.510, but volcanic glasses are the most likely source of humps in the approximate 1.590-1.635 RI range.

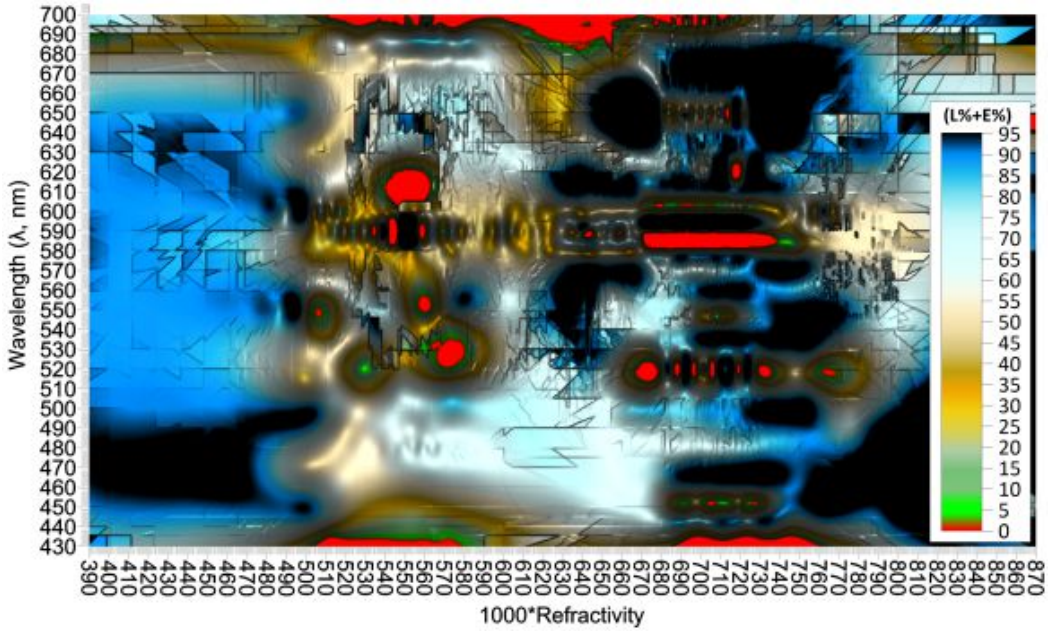

Fig. 3. The Statistical-Density-Function (E%) and Cumulative-Frequency-Distribution (L%) surfaces are added for the 95.22% transparent fraction of the model, (L%+E%) capturing all of the RI signal in one statistic. Later work agrees better with Dr. Macdonald's "iron ore (4%)" estimate of opaques.

The most interesting part of the 3D mapping in Figure 3 is in the region of the Augitic Clinopyroxenes called Pigeonite (Fig. 2), where the black and red bands lie in what can be thought of as the lips of an abstract face. These bands are split right down the center by the Fraunhofer Na D line and fall between lines of data at the 580 nm and 600 nm wavelengths. This seems to be due to the magnetics and spintronics of the Zeeman Effect.

A similar but not so obvious effect can be seen in the Forsteritic Olivine region as well. But no such effect is found in the nonmagnetic region of the Salic (dielectric)

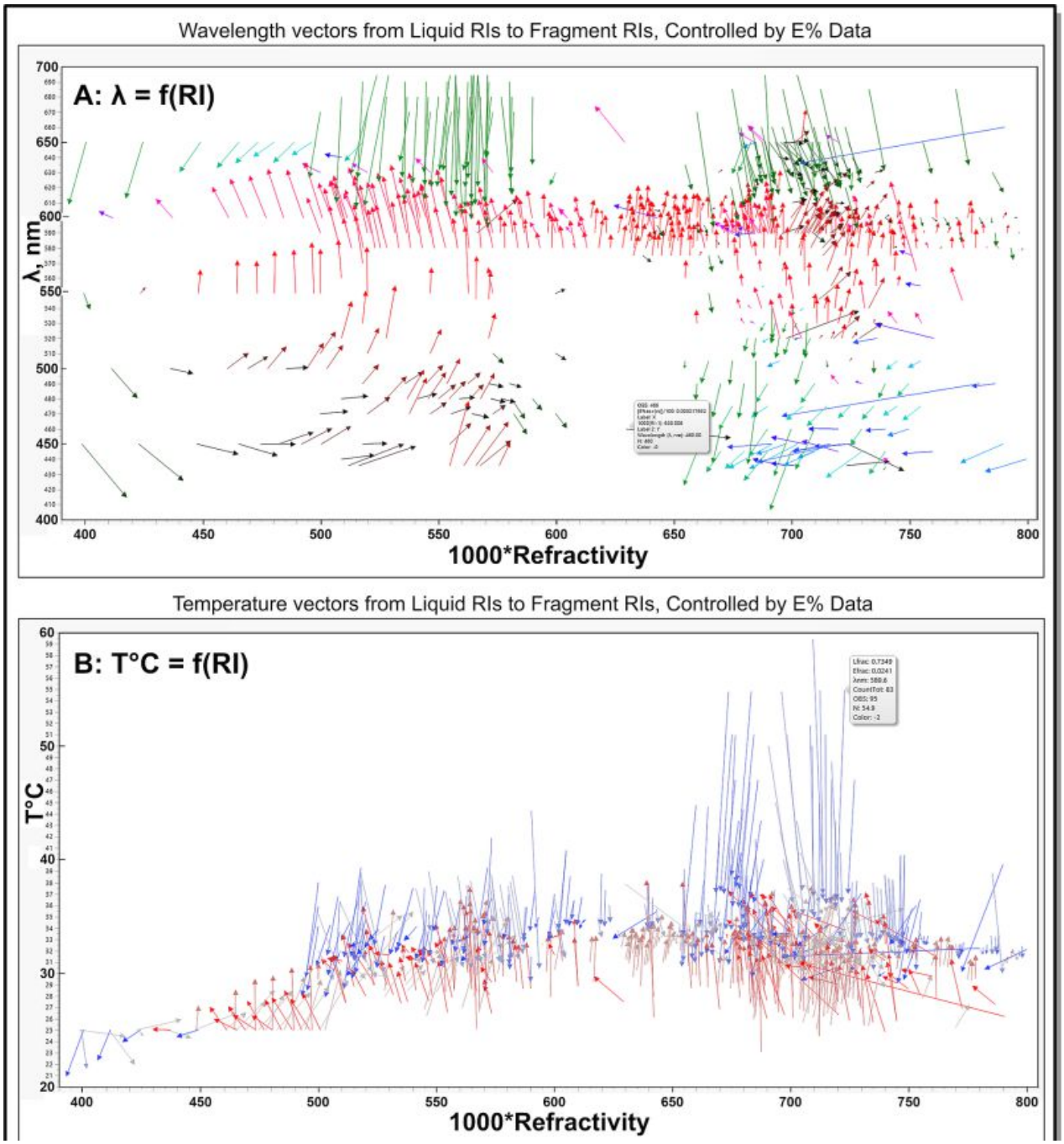

Fig. 4. The backwards calculations of Wavelengths (A), and of Temperatures most resonant among fragment suites (B), were accomplished with the kind help of Laura Archer and the free use of the JMP statistical software, courtesy SAS Academics. Vector bases indicate stage settings for transmitted wavelengths (A) and for thermistor temperatures (B) assumed to be the same as liquid temperatures. Vector tips indicate strongest wavelength or temperature resonances for each suite of particles, case by case.

minerals. Such were the first indications in this work of magnetic "permeability" and electrical "permittivity" (Baker-Jarvis *et al*., 2005; wherein liquid-immersion refractometry is not even mentioned).

The results indicate that liquid-solid boundaries act as transducers. The term "thermalization" seems to account for the temperature effects seen in Figure 4B, but there seems to be no similar term applicable to explain the "weather-like" patterns in Figure 4A. The little boxes of data are included merely to show how one can mouse over vectors to ascertain which case is showing what data.

Note also in Figure 5 that hints of cluster continuity across the 589.3 D line (averaging D1 = 589.6 nm and D2 = 589.0 nm) are few and far between, hampering mineralogical interpretations. However, some patterns at an angle were found in a simpler image, as shown in Figure 6.

The model shown in Figure 7 was formed by adding a model kriged with a 13.5° search ellipse to one with a 103.5° search ellipse. Mappable residuals to that full model are found only in the region of the magnetic, permeability, Femic-mineral fraction. Note also that there is a yellow line showing the bottom of an RI% trench, at the 13.5° angle almost completely separating the Salic from the Femic minerals, as shown in Figure 8.

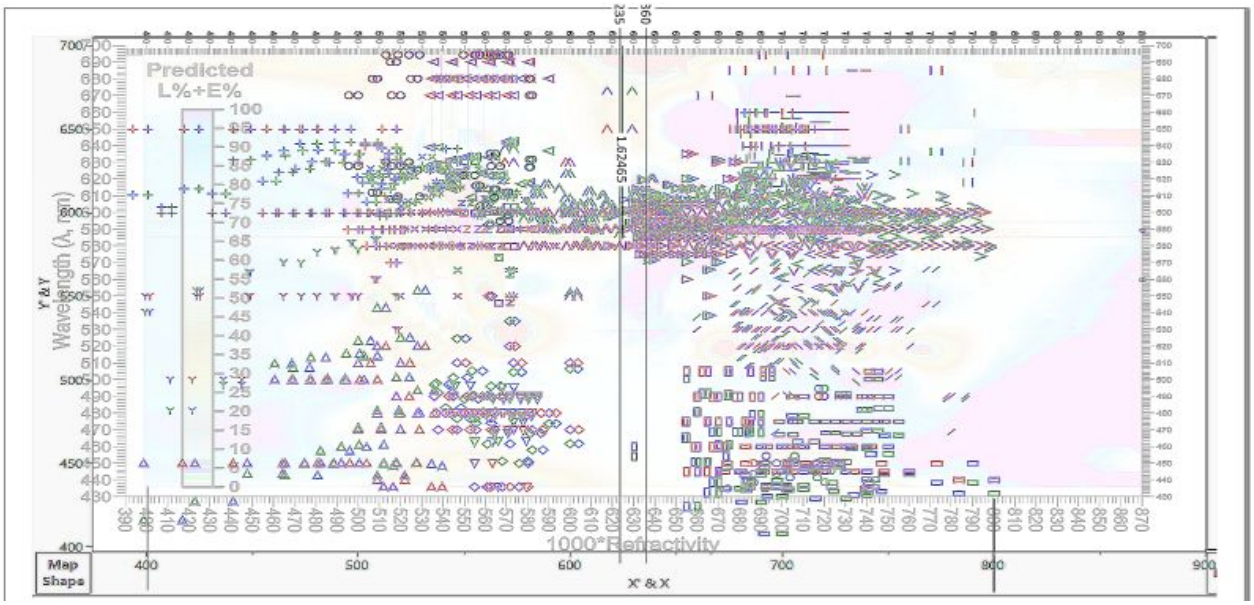

Fig. 5. The concerted efforts to make sense of dendrograms (not shown) and maps (such as this one, created by hierarchical-clustering efforts in JMP) were extremely frustrating. But it turned out to be particularly helpful that clusters were found to be almost completely asymmetric across the Fraunhofer Na D line.

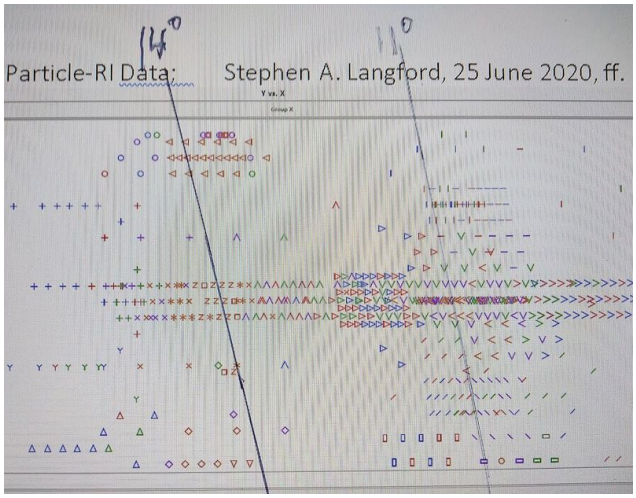

Fig. 6. The alignments across the Fraunhofer D line suggested a krig-modeling search-ellipse rotation.

Several unique mathematical considerations include the fact that *L*%, *E*%, and (*L*% + *E*%) values are almost as precise and accurate as are estimates of immersion-liquid RIs and Wavelength values. Predicted models based upon the Gaussian-distribution assumption, to such heteroscedastic data, are similar to polynomial trend-surface analyses that leave model details unmapped. Uncorrected predicted models tend to have significantly

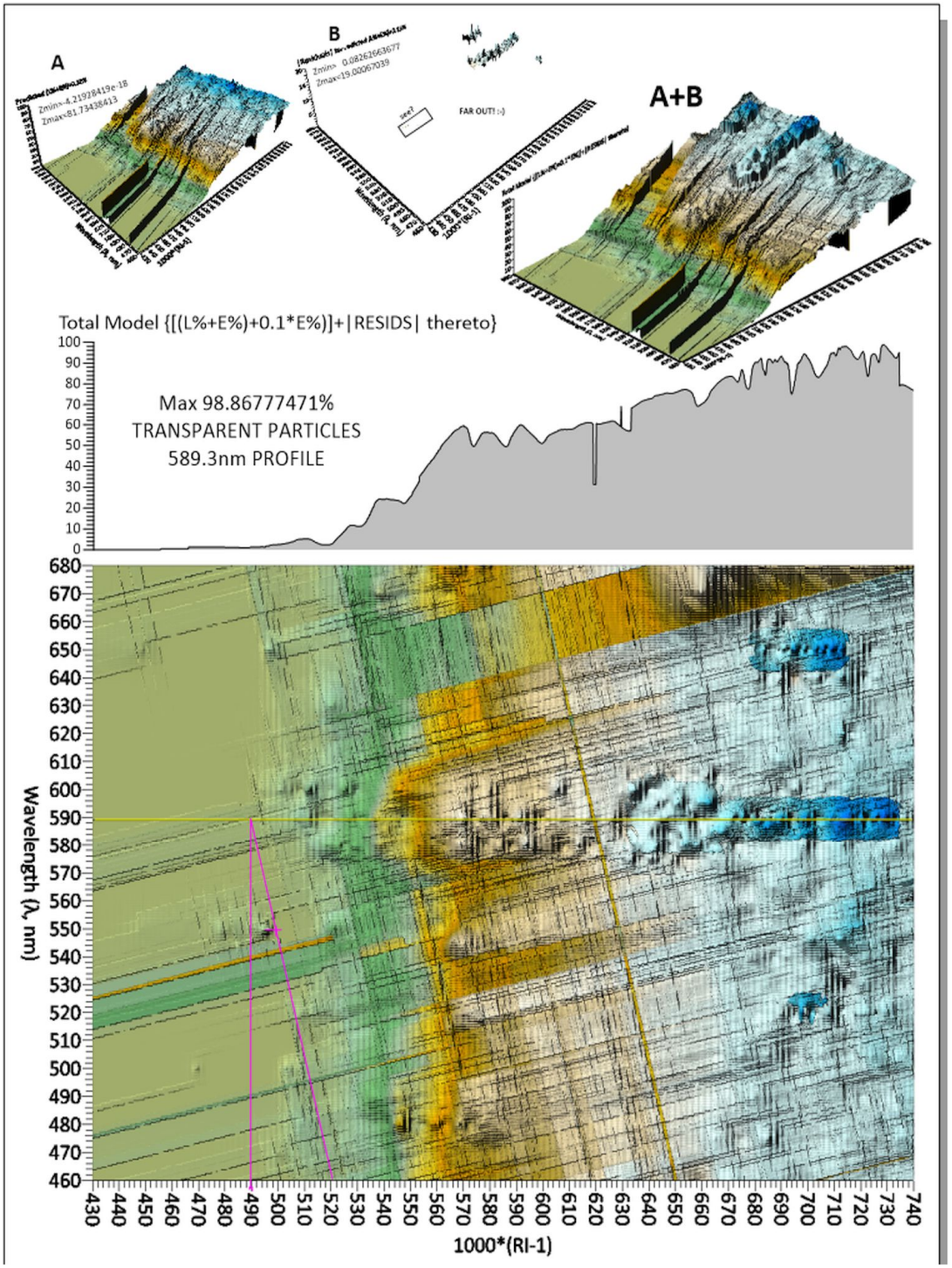

Fig. 7. The cross-kriging of an (L% + E%) model is built from different approaches to each of those two (2) models and includes some extra salting of E%. Note that "RI-terrains" trend separately from X and Y axes but that some features parallel them. Regarding the magenta graphics, note also that any feature's $N_D^{25°C}$ value can be projected along the 13.5° angle to intersect the drawn (yellow) Fraunhofer D line; then to be read at the dropped intersection with the X-axis.

negative minimum-percentage values on the order of a few percent. But adding models of absolute-residual values to those predicted models results in base-level corrections to the same precision level as liquid-RI values have been calculated, as can be seen especially in the video related to the results shown in Figure 9.

Model details have also been increased by adopting innovative approaches such as 1) choosing to model with kriging search ellipses at angles iterated to produce minimal standard errors, 2) choosing to model with various x-band-width choices for search-ellipses, and then 3) using weighted averaging while adding those models together, along with a bit of 4) salting with an extra touch

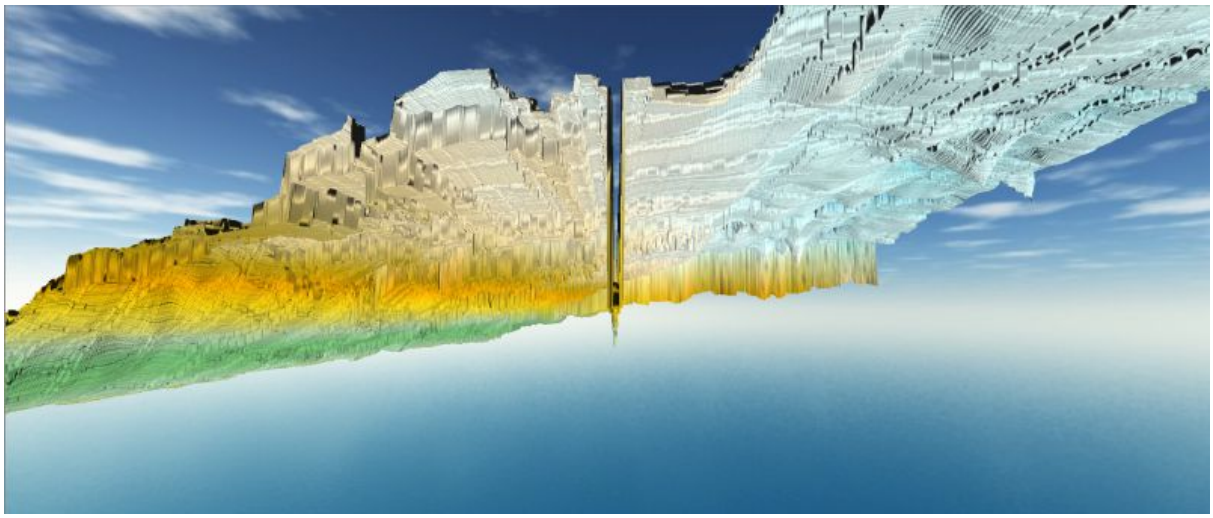

Fig. 8. This striking image, dubbed “Under Spread-Eagle Wings”, shows Salic minerals (at left) and Femic minerals (at right), adjoined by what seems to be a rather tenuous “small body, head, and beak” at the bottom. It is interesting to see bottom views of such models, which are at times more telling than top views.

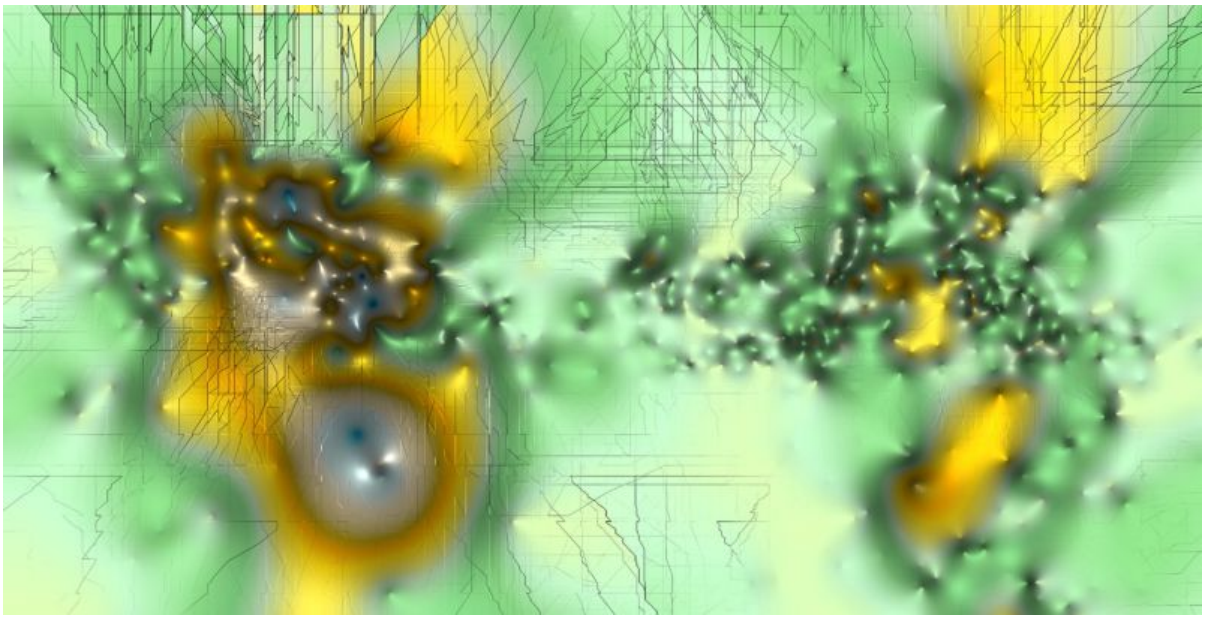

Fig. 9. This is a screenshot of video https://tinyurl.com/v7cys2d, in which the Predicted *E*% model is overlain by the {Total = Predicted + |Residuals|} model. The video loops the Total-Model overlay in and out, showing how adding the |Residuals| adjusts the predicted-model base level from an impossible negative percentage (-%) to a +E-6% (effectively 0%) level, in regions of no data. Note also the Moiré patterns in dense-data areas, as model details are increased and tan-colored areas smooth base levels. *E*% maps [*m*] (mass concentrations related to $E = mc^2$); the shapes are believed to be detailing the EM field.

of *E*%; also, by 5) eliminating vacant modeled areas via addition to them of models kriged with ellipse rotations normal to the first (in particular, here, by adding a model at search-ellipse angle 103.5°, perpendicular to that at 13.5°, to obtain the crosshatched pattern of Figure 7). Such were some of the modeling innovations involved in producing the total model shown in Figures 7 and 8. The grid statistics for that final model are summarized in https://tinyurl.com/y6cmdgu5.

Recent work logs related to calculations of vacuum-structure rest mass (*m*) (https://tinyurl.com/ydxd8goe), energy (*E*) (https://tinyurl.com/y93k9zq3), and weight (*W*) (https://tinyurl.com/ydeqsg5u) have been posted to the ResearchGate databases and might generate future results.

CONCLUSION

The radical, almost-complete separation of Salic from Femic minerals displayed by both Figures 7 and 8 is paradoxical. On the one hand, it looks as though rocks would break most easily between Salic and Femic grains. On the other hand, it shows the strongest "Symphonic Resonances" (coined during this work) obtained during the experiment, seeming to convey the idea that the electric permittivity (ε) and the magnetic permeability (μ) act in unison to hold rocks together, a thought perhaps reinforced by the relationship RI = $n = (\varepsilon\mu)^{1/2}$. It may be that at the granular level the EM fields are strongly holding intermixed grains together; whereas at macro scales related to faulting, Seismologists (if not done already) might want to study whether faults are more likely to occur between surfaces dividing Felsic from Mafic rocks. After first rotating search ellipses by 13.5°, later work isolated the need for another 19.5° rotation, best to fit the strongly magnetic Femic-Residuals data. Searching online for where else 19.5° may have been found to be important led to the amazing finds at http://marcelvogel.org/sacredgeometry.htm.

ACKNOWLEDGEMENT

Comprehensive acknowledgments are provided at https://tinyurl.com/qt20n48o.

REFERENCES

Baker-Jarvis, J., Janezic, MD., Riddle, BF., Johnk, RT., Kabos, P., Holloway, CL., Geyer, RG. and Grosvenor, CA. 2005. Measuring the Permittivity and Permeability of Lossy Materials: Solids, Liquids, Metals, Building Materials, and Negative-Index Materials. NIST Technical Note 1536, Electromagnetics Division. pp 172. https://nvlpubs.nist.gov/nistpubs/Legacy/TN/nbstechnicalnote1536.pdf

Emmons, RC. 1943. The Universal Stage (With five axes of rotation). Geol. Soc. Am. Memoir 8, Judd and Detweiller, Washington, DC., USA. pp 205. http://memoirs.gsapubs.org/content/8 and http://tinyurl.com/oz98vpu

Langford, SA. 1972. Statistical method in optical crystallography: Technique and application to rock forming minerals. Ph.D. dissertation, University of Hawaii, Hawaii, USA. pp 185. https://scholarspace.manoa.hawaii.edu/bitstream/10125/11643/1/uhm_phd_7315944_r.pdf

Langford, SA. 1982. Refractive-index profile of a tephra sample from the 18 May 1980 eruption of Mt. St. Helens. The Microscope. 30:81-91.

Langford, SA. 1991. A modified Jelley refractometer. The Royal Microscopical Society J. Microscopy. 163(September, Part 3):333-345. https://onlinelibrary.wiley.com/doi/pdf/10.1111/j.1365-2818.1991.tb03184.x and https://tinyurl.com/ya9ahlc8

Macdonald, GA. 1942. Petrography of Maui. Hawaii Div. Hydrog. Bull. 7(Part 3):276-334.

Saylor, CP. 1935. Accuracy of microscopical methods for determining refractive index by immersion. J. Res. Nat. Bur. Standards. 15:277-294.

Received: Jan 2, 2021; Accepted: Feb 1, 2021